Asociación Argentina
de Mecánica Computacional

Mecánica Computacional Vol XXVII, págs. 1193-1203 (artículo completo)
Alberto Cardona, Mario Storti, Carlos Zuppa. (Eds.)
San Luis, Argentina, 10-13 Noviembre 2008

SIMPLE APPLICATION OF OPEN SOURCE PIV TECHNIQUE FOR MEASURING DISPLACEMENTS AND STRAINS

Gustavo M. Castelluccio[a], Richard. E. Bravo[b], Hugo A. Ernst[b], Alejandro A. Yawny[c] y Juan E. Perez Ipiña[d]

[a]*PhD student at Georgia Institute of Technology, Atlanta, GA, USA. castellg@gatech.edu*
[b]*Department of Structural Integrity, TENARIS Dr. Simini 250, Campana, Buenos Aires, Argentina*
[c]*Grupo física de metales, Inst. Balseiro. Av. Bustillo 9500 (8400) Bariloche, Río Negro, Argentina*
[d]*Grupo Mecánica de Fractura, Universidad. Nacional del Comahue, Buenos Aires 1400 (8300), Neuquen, Neuquen, Argentina*

Keywords: Inhomogeneity, PIV, image correlation.

Abstract. Strain measurements obtained from images can be useful in the study of constitutive equations or cracks stress concentration among other open problems. Many techniques have been used to calculate the deformation between to images, but they generally require complex or expensive software applications. In this work an open source code for Particle Image Velocimetry under MATLAB© (MATPIV) was employed to measure strains around 10% in uniaxial deformation. A regular pattern was drawn on the surface of a tensile specimen which was observed and deformed simultaneously inside the chamber of a Scanning Electronic Microscope. A posteriori analysis of the images using the code MATPIV allowed computing the strains of an inhomogeneous welded material. These values were compared with direct measurements of the deformed pattern and good agreement was obtained. Moreover, small cracked fracture specimens were also analyzed, but difficulties aroused due to large displacements and rotations. However, a displacement field was calculated by measuring directly the position a regular grid. Then, the strain field under the large deformation model was obtained with a simple numerical scheme.

INTRODUCTION

1.1. Small scale tests

In the last decades improvements in experimental techniques have allowed to characterize materials mechanical properties at smaller scales. One of these methods consists of deforming a small specimen inside a Scanning Electron Microscope (SEM) while images of the surfaces are captured. As a result, the behavior of the material can be studied at a micrometer scale. However, smaller scales require new strategies to measure physical magnitudes, for instance displacements or strains. Since this information is embedded in the images captured, an appropriate analysis is required.

A myriad of mathematic tools can be employed to acquire physical information from images; Fourier analysis, wavelets or simple correlations are among the most common ones. The choice may depend on the physical behavior of the problem (i.e. if some type of function is expected to describe the problem), previous background or available tools.

The analysis using crosscorrelation of images has been widely employed and there are many commercial software applications that calculate the displacement field based on images. Moreover, some open source scripts are available and they provide the chance to modify the algorithm. In the following section some basic concepts regarding the crosscorrelation of images are presented. This method will be afterwards applied to analyze the mechanical test of weld.

1.2. Particle Image Velocimetry (PIV)

PIV is a popular method for measuring displacement fields in fluids mechanics. It is based on pattern matching of two successive images of a fluid with suspended particles. This technique is as a generic tool to measure displacements and, in essence, it does not depend whether images correspond to fluids or solids. Hence, it can be a useful tool to analyze inhomogeneous deformation of solids.

1.2.1. *Pattern matching (Sveen J. K, 2004)*

The displacements in a flow or body can be inferred from two consecutive images of it (I_1 and I_2). By dividing both images into smaller regions or sub-windows, each sub-window in the first image can be compared with a sub-window in the second image. Let $I_1^{i,j}$ denote the sub-window number *i,j* in the first image and $I_2^{i,j}$ the corresponding sub-window in the second image. It is possible to estimate the displacement of the pattern in $I_1^{i,j}$ by evaluating the squared Euclidean distance between the two sub-windows. This is,

$$R_e(s,t) = \sum_{m=0}^{M-1}\sum_{n=0}^{N-1}\left[I_1^{i,j}(m,n) - I_2^{i,j}(m-s,n-t)\right]^2 \qquad (1)$$

For every possible overlap of the sub-windows, it can be calculated the sum of the squared difference between them. Hence, this is a criterion to define the position where the subwindows are the “least unlike”. Expanding the previous equation it is obtained,

$$R_e(s,t) = \sum_{m=0}^{M-1}\sum_{n=0}^{N-1} I_1^{i,j}(m,n)^2 - 2I_1^{i,j}(m,n)I_2^{i,j}(m-s,n-t) + I_2^{i,j}(m-s,n-t)^2 \qquad (2)$$

Notice that the first term, $I_1^{i,j}(m,n)$ is just a constant since it does not depend on *s* nor *t*. The last term, $I_2^{i,j}(m-s,n-t)^2$, depends on *s* and *t*, but varies only with the second image. Consequently, only the middle term actually deals with both our images. Moreover, it is proportional to the function

$$R_e(s,t) = \sum_{m=0}^{M-1}\sum_{n=0}^{N-1} I_1^{i,j}(m,n)\cdot I_2^{i,j}(m-s,n-t) \tag{3}$$

which is usually referred to as the cross-correlation.

The basic assumption here is that the pattern in $I_2^{i,j}$ is evenly distributed so that the sum of $I_2^{i,j}()^2$ does not change as we vary *s* and *t*. Further details can be found in (Sveen J., 2004).

1.3. Inhomogeneous materials

The characterization of inhomogeneous materials is a complex task in part because many length scales are involved. In the case of fusion welds, some portion of the metal achieves the liquid state and solidifies producing an inhomogeneous region. Moreover, the surrounding material suffers the influence of the heat diffused and becomes the so called Heat Affected Zone (HAZ). The HAZ extends a few millimeters from the liquid-solid interface into the original metal and has a steep gradient of mechanical properties.

Tensile properties of the HAZ cannot be measured with standard procedures due to its small dimensions but they can only be estimated with indirect methods. However, these properties are of significant importance for girth welds because they may determine the failure stress of a structure.

The behavior of the HAZ in the presence of a crack is also a tough task to describe. The inhomogeneity of the HAZ make traditional fracture mechanics methodologies invalid and thus strains around the crack do not follow the traditional HRR field (Anderson, 1995). Moreover, if small specimens are employed, additional differences with the HRR model may arise, even for homogeneous specimens. In this case experimental results can be useful to calibrate fracture mechanics numerical models.

These characteristics suggest that small scale tests can be adequate to study the HAZ.

1.4. Objective

This work explores how to calculate strains from images of the Heat Affected Zone of a weld. The images correspond to small specimens with grids on their surfaces that were deformed inside a scanning electron microscope (SEM). Tensile specimens and bending cracked specimens were studied using the PIV algorithm previously described.

Alternatively, strains were estimated by measuring directly the displacement of a grid and using large deformation formalism.

2. EXPERIMENTAL DETAILS

2.1. Material and welds

The material studied was extracted from a pipe with yield strength around 470MPa and ultimate tensile strength of around 570 MPa. Two segments of pipes were welded and the resulting weld metal had a higher strength (overmatch).

A weld bevel with a straight side, usually called “K”, was used to analyze only one microstructure along the thickness of the specimen.

2.2. In Situ Test

In-situ tests are mechanical tests performed inside the chamber of a SEM. This technique allows a direct observation of the sample while it is loaded and deformed. The specimen and the testing machine work under the vacuum of the chamber, and access is restricted during the test.

The testing machine consists of two mobile heads that can stretch or compress the specimen under displacement control. Using appropriate grips, tensile tests and fracture toughness tests may be carried out. Further details can be found in Yawny et al 1997.

2.3. Samples

Space available inside the SEM chamber is limited and allows the use of small samples only, see Figure 1. The weld and HAZ regions are located within the sample.

Regular grids were drawn on the surface of the samples in order to visualize the resulting deformation. Similar solutions have already been developed in recent literature (Biery et al, 2003).

The width of the tensile sample is limited by the maximum load that can be applied by the machine. Specimens were obtained in the transverse direction to the weld and included base metal, welded metal and HAZ.

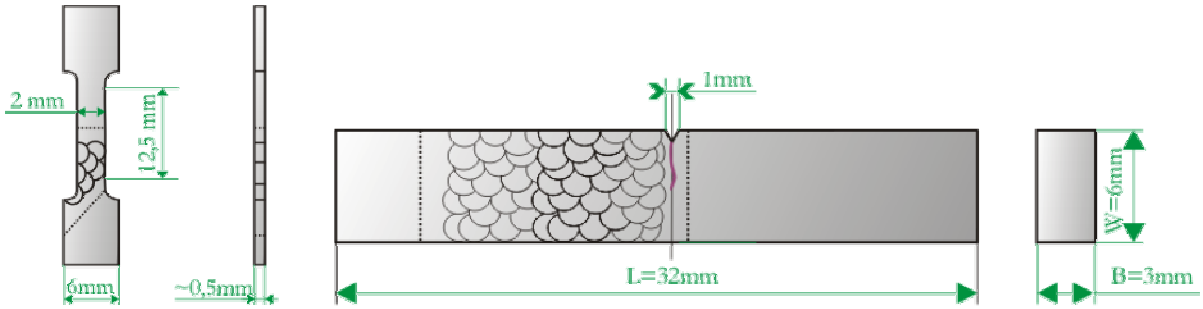

Figure 1. Small samples used in the in situ tests.

Three point bending samples were machined from the welded pipes and fulfilled BS 7448 Part 2 (1997) recommendations except for dimensional requirements. A narrow fatigue crack was generated in the coarse grain zone of the HAZ (CGHAZ).

After polishing and etching the surfaces, the crack and the fusion line were located. Figure 2 shows the specimen as observed with the SEM and a detail of the crack seen with an optical microscope. The crack was located in the CGHAZ, less than 150 µm from the fusion line. Furthermore, since the width of the sample is only 3 mm, it is not expected that the position of the crack vary significantly from the fusion line inside the specimen.

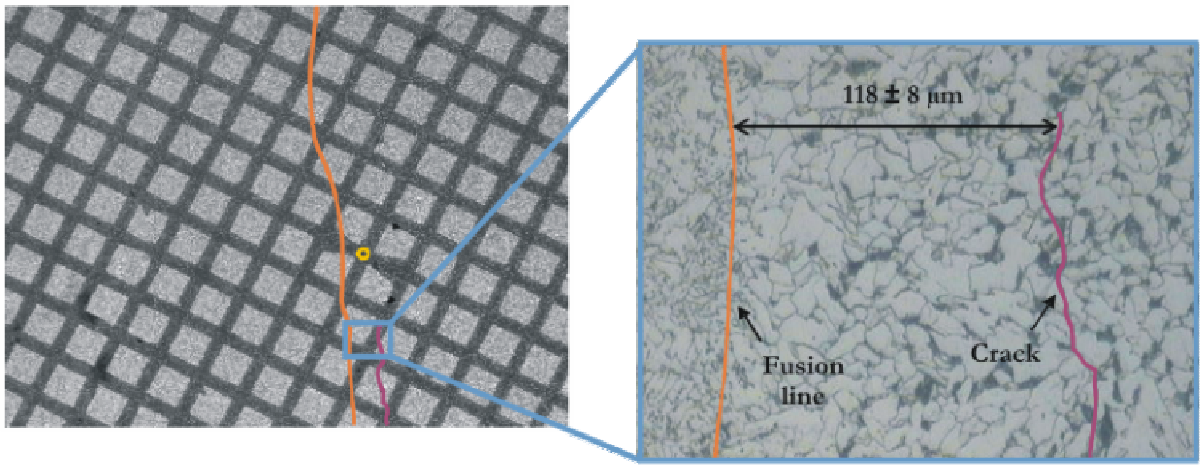

Figure 2. Location of the crack near to the fusion line.

3. ANALISIS OF THE IMAGES AND RESULTS

The analyses of the images obtained during the tests are described in this section. In the first two subsections, the PIV algorithm previously described was employed to analyze images from tensile tests. It was showed that a regular grid can introduce spurious, so a different strategy is proposed in the last two subsections to study the strains around cracks.

3.1. Tensile properties

During the tensile tests samples were deformed to failure and loading was stopped to record pictures. Images in Figure 3 were obtained during the tensile tests of the HAZ.

Fusion line was located using micrographs from an optical microscope, and it was highlighted on the photographs. Notice that the welded metal had no apparent deformation, while the HAZ suffered some stretching. Thus, the HAZ has lower yield strength than the weld metal. This fact correlates well with hardness measurements (not presented here).

The engineering strain at a load of (448±4)N was estimated by measuring the length of the grid squares. The result indicated that the maximum deformation reached in the HAZ was 12%. Afterwards, the sample broke far from the fusion line due to problems in the grip

Note that for every image the strain and stress can be measured and thus contribute with a point for the stress-strain diagram.

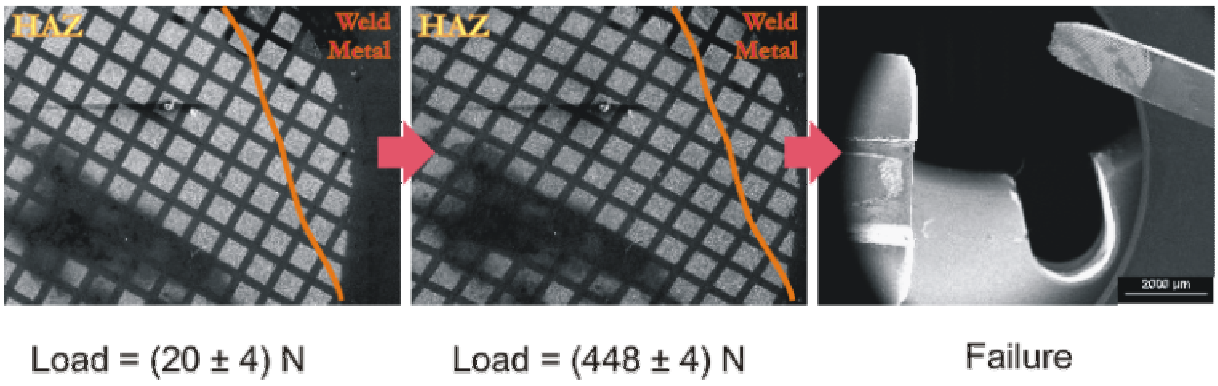

Figure 3. Images taken with the SEM during the test of HAZ. Note how the squares are deformed. Fusion lines are drawn over the pictures.

3.2. PIV analysis

Open libraries from the MATPIV project were adapted for measuring strains on the images. This project is an application of the PIV theory using MATLAB scripts. The libraries are free under the term of the GNU General Public License, and scripts are open to be modified. It should be emphasized the conveniences of using these libraries, which are available online, have tutoring information and can be easily modified.

Though PIV is usually employed with random patterns, its theoretical bases are applicable to a regular grid like the one on the specimens. Thus, it was necessary to evaluated if MATPIV could be applied to this grid. It was found that the software works fine for displacements smaller than the period of the grid, but for displacements close to the period of the grid, MatPIV adds spurious displacements of around the period of the grid (see Figure 4).

Luckily, this lack of accuracy can be easily detected but difficult to be corrected, so it was avoided to analyze images which had displacement around or larger that the grid period. Moreover, it was chosen to use the *multin* option from *MATPIV* that provided the best results. With this option the calculation starts with relatively large subwindows and refines the calculation using smaller windows. Based on trial and error it was preferred a final window size (after refinement) of 192x192 pixels, that provided a resolution in the displacement of 70μm while saving enough information on each subwindow to calculate accurately the crosscorrelation. Strain fields were calculated using the *strain* subroutine in MATPIV. In particular, the *circulation* option was employed, which is based on the Sobel´s algorithm to recognize gradients.

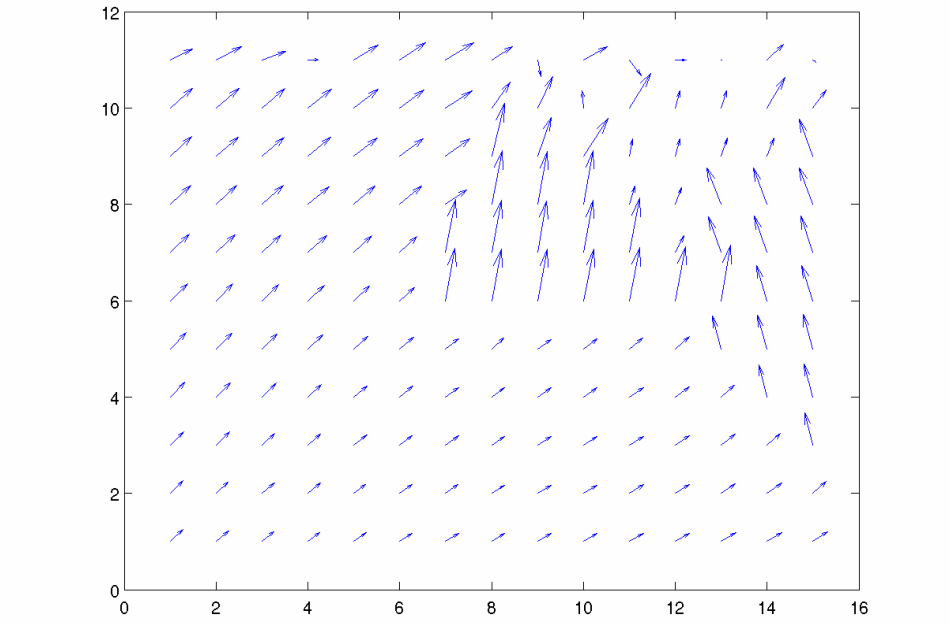

Figure 4. Spurious displacements due to the large displacements between the images.

Figure 5 presents the strain field measured for the boundary between the weld metal and the HAZ. Only the upper part of the image that is not blurred by oxides is considered.

The fusion line was located using micrographs and it coincides with the region with the steepest gradient of strains.

The largest deformation appears in the HAZ, while the welded metal seems to be in the elastic regime. Using an average value of the strain and the loads measured experimentally, the strain stress curve can be obtained.

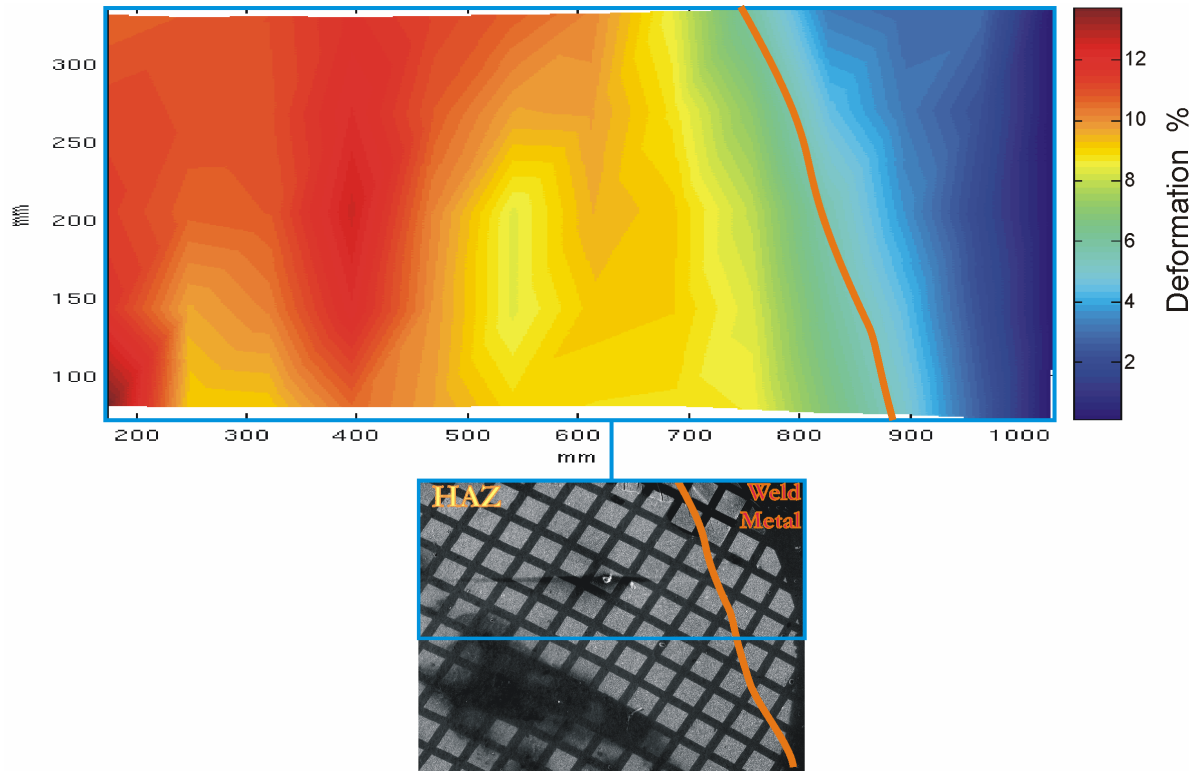

Figure 5. Measured strains for the tensile specimens.

3.3. Strains around a crack in the HAZ

Three point bending specimens were deformed inside the SEM while observing the surface of the sample. Two type of images were obtained, one of low magnification (11X), and others of high magnification (101X). From the higher magnification pictures, CTOD can be directly measured. Figure 6 gives an example of the two types of images.

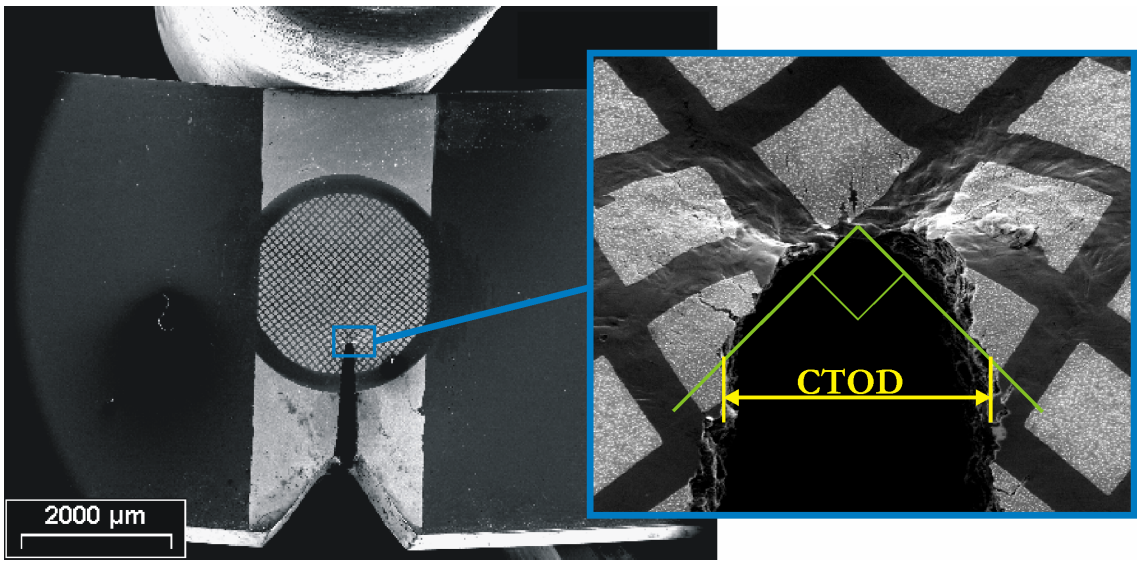

Figure 6. On the left a picture of the sample with low magnification. On the right a detail of the tip of the crack and the CTOD.

3.4. Large deformation analysis

The grid on the surface of the specimen was used to measure local deformations. Large displacements and strains are involved and make the small strains approximation invalid. Thus, finite strains and deformations theory needs to be applied. Two classes of definitions are generally used: strains defined in the undeformed configuration, usually called Lagrangian formulation, or strains based on the deformed configuration, Eulerian formulation.

The Eulerian formulation was chosen to describe displacements; each point in the deformed picture is associated to a stain value. This leads to represent strains with the Almansi strain tensor (Malvern, 1969), defined as:

$$E_{ij}^{*} = \frac{1}{2}\left[\frac{\delta u_i}{\delta x_j} + \frac{\delta u_j}{\delta x_i} - \frac{\delta u_k}{\delta x_i}\frac{\delta u_k}{\delta x_j}\right] \tag{4}$$

Small strain hypothesis neglects the non-lineal term in equation (2). The Almansi strain tensor is not just a second order approximation, but describes completely the problem.

PIV method was tested but no satisfactory results were obtained due to the large deformations, rotations and roughening of the surface. Consequently, it was preferred to obtain displacements by measuring directly the coordinates –in pixels- of the corners of the squares (a similar solution was proposed by Schroeter, 2001). In other words, the images are mathematical functions with a discrete domain of pixels. One material point does not have the same coordinate in the initial and final images due to the rotation and displacements of the specimen. Thus, the following two coordinate systems can be defined:

Coordinate system of the initial image: ${}^{0}z_i$, $i = 1,2,3$

Coordinate system of the final image: ${}^{f}z_i$, $i = 1,2,3$

Each square of the grid was parameterized using a set of convective coordinates (r,s) as shown in Figure 7. This figure presents a square before and after being deformed.

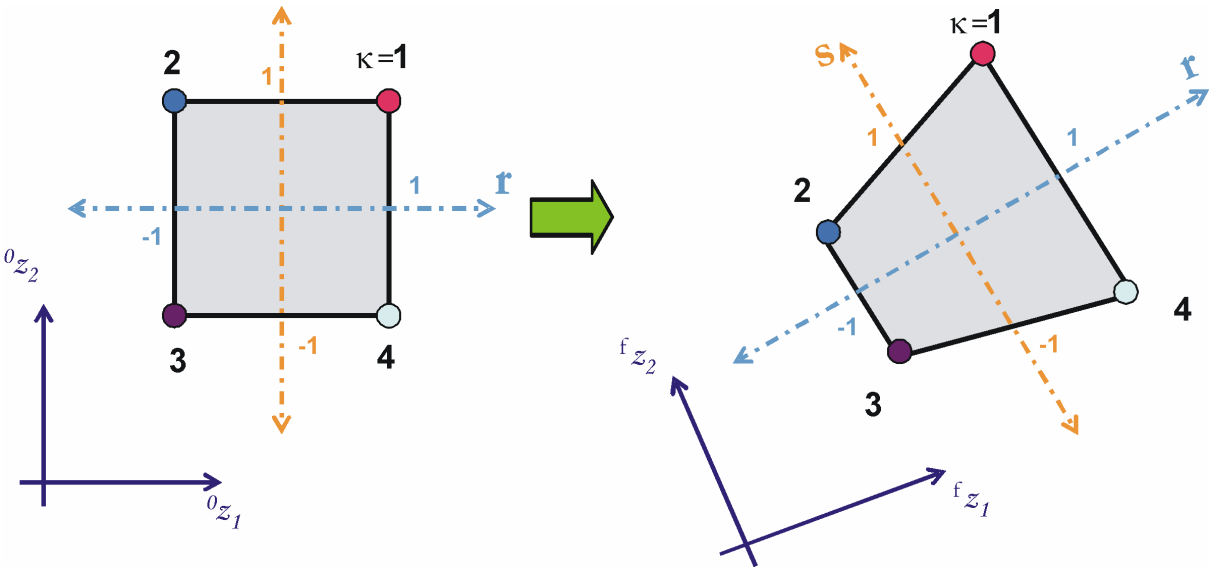

Figure 7. Initial (Lagrangian) and final (Euclidean) coordinate systems along with the parameterization of the convective coordinates.

Traditional parametric interpolation functions were used, defined as:

$$ {}^{t}z_i(r,s) = h(r,s)_k \, {}^{t}z_i^k \tag{5} $$

where t refers to the image and k summation of the linear interpolation functions that are defined as:

$$ h_1 = \frac{1}{4}(1+r)(1+s), \quad h_2 = \frac{1}{4}(1-r)(1+s), \quad h_3 = \frac{1}{4}(1-r)(1-s) \quad \text{and} \quad h_4 = \frac{1}{4}(1+r)(1-s) \tag{6} $$

This methodology assumes that the squares deform with rigid straight sides. This is an approximation that, in general, proved to be adequate to the experimental uncertainties, except maybe for some squares close to the crack tip. I this latter case, the squares could be divided into smaller ones to increase the accuracy.

The deformation gradient inside each square was calculated using:

$$ {}^{f}_{0}X = \frac{\delta {}^{f}z_i}{\delta {}^{f}z_j} = \frac{\delta h_k}{\delta {}^{f}z_j} \, {}^{f}z_i^k \tag{7} $$

using the parametric interpolation function

$$ \frac{\delta {}^{0}z_i}{\delta r} = \frac{\delta h_k}{\delta r} \, {}^{0}z_i^k \quad \text{and} \quad \frac{\delta {}^{0}z_i}{\delta s} = \frac{\delta h_k}{\delta s} \, {}^{0}z_i^k \tag{8} $$

and defining the Jacobian matrix as:

$$ \left[{}^{0}J \right] = \begin{bmatrix} \dfrac{\delta {}^{0}z_1}{\delta r} & \dfrac{\delta {}^{0}z_2}{\delta r} \\ \dfrac{\delta {}^{0}z_1}{\delta s} & \dfrac{\delta {}^{0}z_2}{\delta s} \end{bmatrix} \tag{9} $$

it is deduced that:

$$ \begin{bmatrix} \dfrac{\delta h_k}{\delta {}^{0}z_1} \\ \dfrac{\delta h_k}{\delta {}^{0}z_2} \end{bmatrix} = \left[{}^{0}J \right]^{-1} \begin{bmatrix} \dfrac{\delta h_k}{\delta r} \\ \dfrac{\delta h_k}{\delta s} \end{bmatrix} \tag{10} $$

Combining this result with equation 8, the deformation gradient was found (Dvorkin 2006).

This calculation scheme was implemented in Matlab and the Almansi strains principal values were found for each square of the grid.

Results for one image for the Base Metal and the HAZ specimen with HI 0.8 kJ/mm are presented in Figure 8 and Figure 9. Here the Almansi strain tensor is plotted in its principal coordinates.

For the Base Metal specimen, strains measured at the surface are approximately symmetric to the crack. Intense compression strains are found in the through thickness direction (around 30%). In front of the crack tip, along the direction that might follow the crack, strains are lower than 5%.

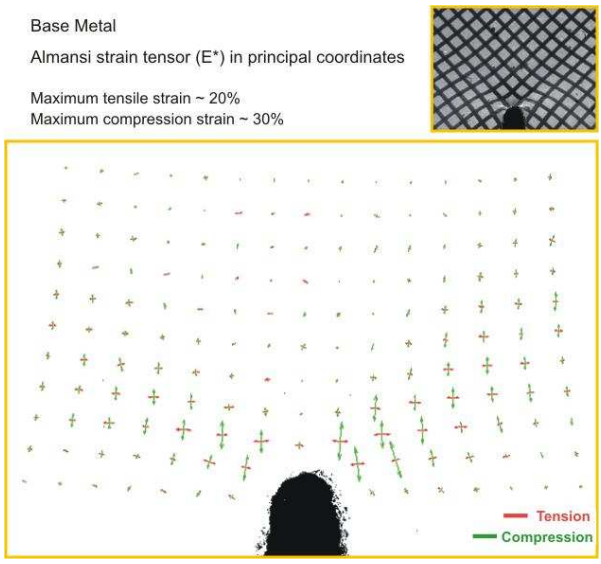

Figure 8. Large deformation analysis of the crack tip for the base metal. Approximately symmetric strains are found in front of the crack.

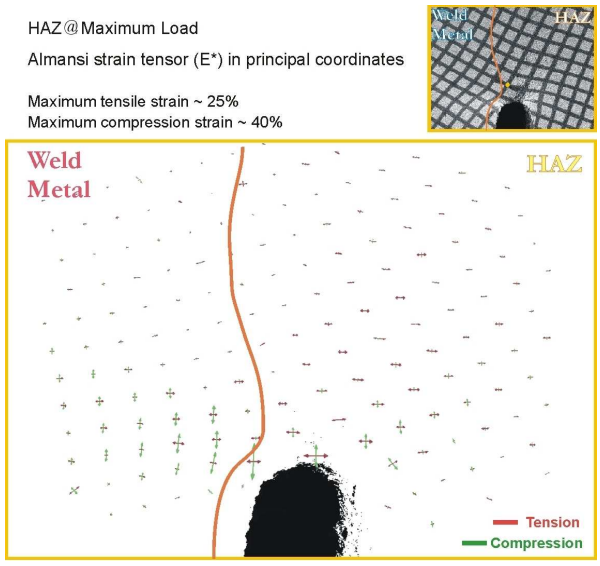

Figure 9. Large deformation analysis of the crack tip for the weld. Note the highly asymmetric strains that are encountered.

In the HAZ specimen, intense compression strains were found along the crack growth direction, especially in the weld metal region. There was no significant deformation in the path followed by the crack and strains decreased steeply and become fewer than 5% at a distance smaller than the CTOD. Asymmetry was found in the strain field as a consequence of the interface between the base metal, welded metal and HAZ. These results can be useful as an input for fracture mechanics models of inhomogeneous regions.

4. SUMMARY AND CONCLUSIONS

MatPIV, which are open source scripts for PIV analysis, were successfully implemented to calculate displacements and strains of images of a specimen obtained during a tensile test. In particular, this method allowed to measure mechanical properties from small regions of an inhomogeneous material.

Moreover, surface deformation of cracked three point bending specimens was calculated by direct measurement of a grid. The asymmetry in the strain due to the weld metal HAZ interface was proved and can be applied to calibrate other numerical fracture models.

ACKNOWLEDGEMENTS

The first author would like to thank Eduardo Dvorkin for his support regarding the large deformation formulation and the Roberto Rocca Program for sponsoring his fellowship at Georgia Tech.

REFERENCES

Anderson T. L.. Fracture Mechanics. Fundamentals and Applications. CRC. Press, 2 edition, 1994.

Biery N, de Graef M. and Pollock T. M. A method for measuring microstructural-scale strain using a scanning electron microscope: Application to γ-titanium aluminides. Metallurgical Transactions A, 34A:2001–2313, October 2003.

BS 7448: Part 2. British Standard. Part 2: Fracture mechanics toughness test. 1997.

Dvorkin E. Cálculo de deformaciones a partir del grillado. Private comunication, 2006.

Malvern L. E. Introduction to the Mechanics of a Continuous Medium. Prentice-Hall, 1969.

Schroeter, B. Measurement of Inhomogeneous Deformation Fields in Polycrystalline OFHC Copper. Master thesis in mechanical engineering, Georgia Institute of Technology, 2001.

Sveen J. K. An introduction to matpiv v.1.6.1. Eprint no. 2, ISSN 0809-4403, Dept. of Mathematics, University of Oslo, 2004. http://www.math.uio.no/~jks/matpiv

Yawny A. J. Malarría, E. Soukup, and M. Sade. Stage for in situ mechanical loading experiments in a scanning electron microscope (Philips 515) with a small chamber. Review Scientific Instruments, 68(1):150–154, January 1997.